NUMERICAL AND EXPERIMENTAL ANALYSIS OF CRACKS AND FAILURE MODE OF CONCRETE BLOCK PRISMS

M.A. Ramalho[1] and A. Taliercio[2]
[1] Professor, Department of Structural Engineering, University of São Paulo, Brazil, ramalho@usp.br
[2] Professor, Department of Civil and Environmental Engineering, Politecnico di Milano, Italy, alberto.taliercio@polimi.it

ABSTRACT
This paper presents a comparison between experimental and numerical analysis of concrete block prisms under compressive loads. The main goal of the study is to compare damage obtained using a numerical non-local damage model specially developed for quasi-brittle materials with the cracks observed in an experimental program. First, blocks and mortar specimens are submitted to compression and direct tension tests in order to identify their damage parameters. Then, prisms are also tested to evaluate their behavior. All the tests are carried out with displacement control to obtain the complete load-displacement diagram for the specimens: the initial linear behavior, the failure load and the post-peak softening branch. After the experimental program, numerical models are developed, using eight-node 'brick' finite elements with secant stiffness matrix. An increasing displacement is applied to the model to simulate the tests. Finally, the cracks and failure mode obtained experimentally are compared with a scalar measure of the damage obtained with the numerical models. Obtained results show that the non-local damage model considered in this paper is able to predict the cracks and even the failure mode of the prisms observed in the experiments.

KEYWORDS: structural masonry, prisms, compression, damage model

INTRODUCTION
A peculiarity of hollow concrete block masonry is that its failure mechanism is completely different from classical solid masonry [1]. Failure starts by web cracking in the plane of the wall, in a mechanism similar to deep beam bending. This means that results and models established for solid masonry cannot be simply extended to hollow block masonry. In light of these remarks, it is clear that the availability of reliable theoretical models and empirical formulae is a key issue in the prediction of the global behaviour of structures made of hollow concrete block masonry.

The behaviour of structural elements made of quasi-brittle materials, such as concrete or masonry, beyond the linear elastic range can be described using damage mechanics. Damage consists basically in the formation, growth and coalescence of micro-cracks, which can lead a structural member to failure, and is matched by a loss of stiffness and strength.

Perhaps the first author who formulated the concept of damage as it is currently known was Kachanov [2], with reference to creep-induced damage in metals. Another important contribution can be ascribed to Rabotnov [3], who proposed a damage variable that could be used to reduce

the initial stiffness and strength of the material. Recently, after the formalization of the so-called Continuum Damage Mechanics [4], the development of this research field was quick and varied.

In this work, a numerical model is proposed to simulate and interpret the mechanical response of hollow concrete block masonry prisms submitted to compression tests in the laboratory. The nonlinear behaviour of concrete and mortar is described through a damage model capable of allowing for the damage-induced anisotropy of the materials. Mesh-dependency effects are controlled using non-local strain measures.

MATERIAL CHARACTERIZATION

The characterization of the materials used in this work was accomplished at the Department of Structural Engineering of University of São Paulo (USP). The tests were carried out both on masonry components, blocks and mortar specimens, and on two-block prisms built with the same components. The hollow concrete blocks had a nominal strength of 8 MPa and the dimensions were 140 × 190 × 390 mm (thickness × height × length), Figure 1a. The cylindrical mortar specimens had a radius of 50 mm and a height of 100 mm, Figure 1b. The mortar mix proportions, in volume, were 1:0.5:4.5 (Type ii of BS 5628 1992).

Figure 1: Concrete blocks (a) and mortar specimens (b)

All the axial compression tests on components and prisms were performed with the aim of obtaining the complete force-displacement curve for the specimens, that is, the behavior of the specimens from the initial loading stage until complete failure. Therefore, a hydraulic servo-controlled press under displacement control at 1 μm/s was used. Despite the fact that the press had an internal displacement control, four additional devices for displacement measurement (LVDTs) were also used in all the tests, see Figure 2.

Figure 2: Axial compression tests a) Block; b) Mortar specimen; c) Prism

In order to characterize the units under compression, six concrete blocks were tested. From the obtained load-displacement diagrams it was possible to define a representative (average) behavior for the units. Figure 3 displays all of the experimental results obtained and the representative block diagram that will be adopted in the numerical analysis of the prism, as described in details in a following section.

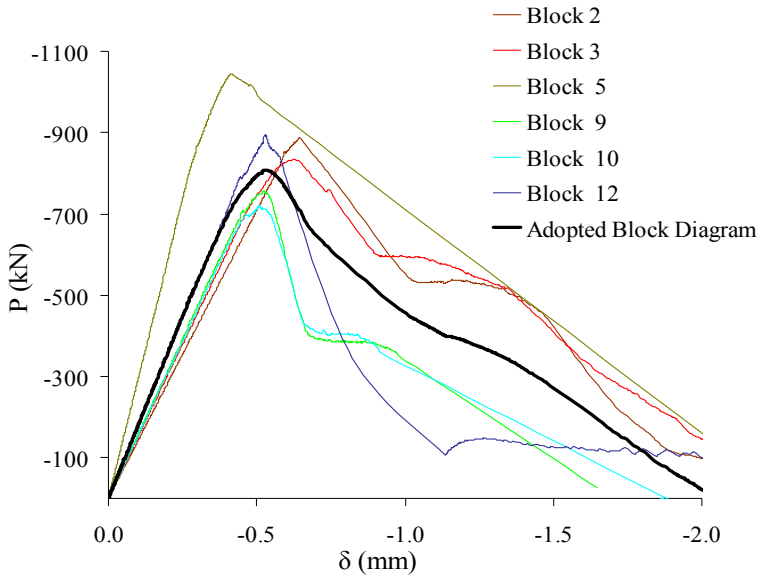

Figure 3: Load-displacement diagrams for blocks with nominal strength of 8 MPa and adopted representative diagram.

As for the tension parameters, a direct tension test was carried out on 20 specimens. The specimen's preparation is shown in Figure 4. The Figure 5 shows the obtained result for the tests and the average diagram which was taken as the representative behavior of the block under tension. This will be used for the numerical prism models, as can be observed in details in a following section.

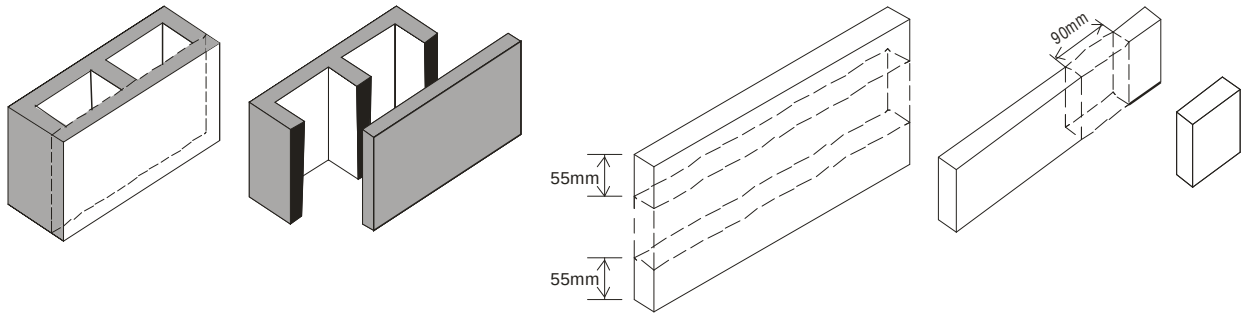

Figure 4: Direct tension – specimens

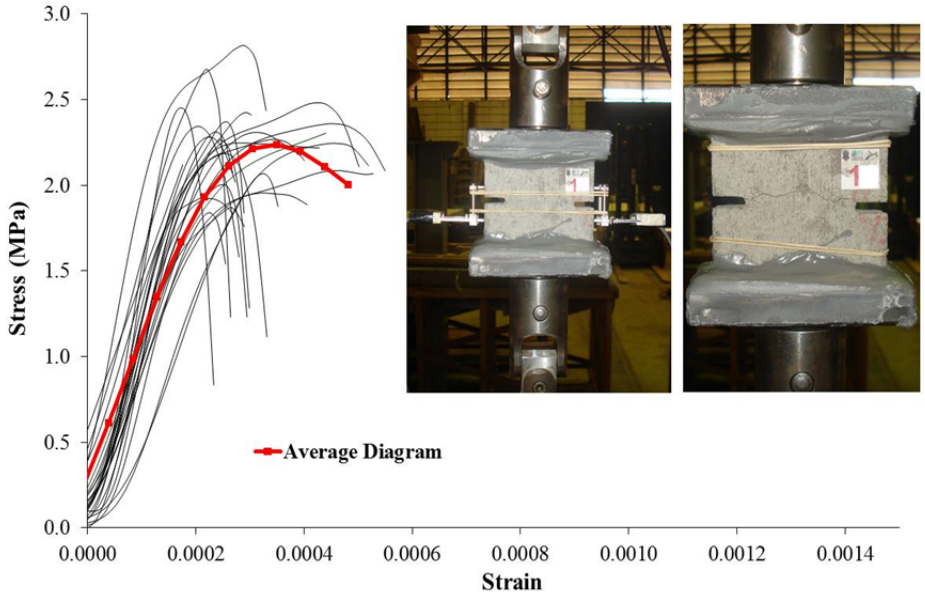

Figure 5: Direct tension test – results and average diagram

DAMAGE MODEL

The model employed in this research was originally developed in [5] to interpret the time evolution of the mechanical damage in quasi-brittle materials, such as concrete and masonry, under either increasing or sustained stresses of high intensity. This model applies to materials which can be assumed to be linearly elastic and isotropic at the virgin (undamaged) state: the Young's modulus and the Poisson's ratio of the material are denoted by E and ν, respectively. The damage phenomena are macroscopically taken into account through a symmetric, second-order tensor $\boldsymbol{D}$. Under increasing loads, provided that creep effects can be neglected, the nonlinear stress-strain law of the material, in finite form, reads:

$$\boldsymbol{\varepsilon} = \boldsymbol{C}(\boldsymbol{D}):\boldsymbol{\sigma} \tag{1}$$

where $\boldsymbol{C}$ is the fourth-order flexibility tensor of the damaged material. The eigenvalues and the normalized eigenvectors of the damage tensor will be denoted by D_α and n_α ($\alpha = I, II, III$), respectively. Note that the damaged material is, in the most general case, orthotropic: n_I, n_{II} and n_{III} are normal to the local planes of material symmetry of the damaged material. Any one of the planes of damage-induced orthotropy is somehow associated to a plane micro-crack that forms in the solid. Once any damage direction is activated, its orientation is supposed to remain fixed throughout the rest of the stress history. Thus, the ensuing model can be qualified as a "non-rotating, smeared crack model".

The damage process driving variable is supposed to be an equivalent strain measure, $y = \frac{1}{2}\,\varepsilon^2$. As the maximum eigenvalue of y attains a critical value (y_{0T} or y_{0C}, according to the sign of the associated strain), the first damage direction (n_I) is activated. An additional damage direction, $\mathbf{n}_{II}$, can be activated in the plane orthogonal to n_I if the maximum direct component of y, that is, $y_{hh} = \mathbf{n}_h\cdot(y\cdot\mathbf{n}_h)$, with $\mathbf{n}^h \perp \mathbf{n}_I$, attains the damage threshold. The third possible damage direction is necessarily $\mathbf{n}_{III} = \mathbf{n}_I \wedge \mathbf{n}_{II}$. In the case of increasing stresses, each principal value of the damage tensor is supposed to evolve according to:

$$D_\alpha = 1 - \frac{1}{1 + A_H \left\langle y_{hh} - y_{0H} \right\rangle^{B_H}},\ \alpha = I, II, III. \tag{2}$$

Here, $\langle * \rangle$ are McAuley brackets and A_H and B_H are material parameters, which take different values according to the sign of the strain component that activates damage (H=T for tension; H=C for compression).

In local damage procedures the consistent damaged tangent or secant matrix is evaluated considering the local strain state. However, in most problems where strain-softening materials are involved, this procedure leads to spurious results and strong mesh sensitivity [6]. Typically, the inelastic strains are concentrated in narrow bands, whereas the major part of the structure remains nearly unstrained. To overcome this drawback, different techniques can be used. In the so-called integral-type models a non-local state variable is computed at any point in the solid as a weighted average of the local state variable over a neighbourhood, or representative volume, of the point being examined [7],[8]. The size of such volume is related to a characteristic length of the material, l_c.

In this paper, similarly to [9], the non-local procedure implemented in the finite element code is based on an integral-type procedure, involving a weighted average of the strain. This procedure was selected as it can be easily implemented in a finite element code. So, the average strain at any point x, which replaces the local strain in the governing equations, is defined as:

$$\boldsymbol{\varepsilon}_a(\boldsymbol{x}) = \frac{\int_V f(\boldsymbol{x} - \boldsymbol{x}_s)\boldsymbol{\varepsilon}(\boldsymbol{x}_s)dV}{\int_V f(\boldsymbol{x} - \boldsymbol{x}_s)dV} \tag{3}$$

where $\boldsymbol{\varepsilon}(\boldsymbol{x}_s)$ is the strain at any source point $\boldsymbol{x}_s$, $f(\boldsymbol{x}\text{-}\boldsymbol{x}_s)$ is a scalar weighting function, and V is the volume of the representative neighbourhood.

Several expressions have been proposed for the weighting function f, which is often assumed to be of the form:

$$f(\boldsymbol{x} - \boldsymbol{x}_s) = \exp\left[-\left\| \frac{\boldsymbol{x} - \boldsymbol{x}_s}{2l_c} \right\|^2 \right] \tag{4}$$

where l_c is the internal length of the non-local continuum, a material property which represents the diameter of a sphere centred at the current point $\boldsymbol{x}$ and defines the size of the localization zone. l_c can be related to the fracture energy of the material [10].

Basically there are two procedures to verify the event of strain localization in the analysis. First, the load-displacement diagram presents a clear discontinuity just after the peak load. Second, the number of iterations increases suddenly for the load step just after the peak load and sometimes it is not even possible to attain any convergence in the procedure. On the other hand, if no strain

localization occurs, the load-displacement diagram does not exhibit any discontinuity and there is no significant difference between the numbers of iterations at the various steps of the analysis.

It is worth emphasizing that the non-local strains are used only to evaluate the flexibility matrix. Stresses are computed according to local strains, as they must be compatible with the real displacement field; otherwise, convergence would not be achieved or, at least, would be hard to obtain. Finally, note that local strains are replaced by average strains only if the material is actually damaged: performing this replacement as long as the material is in the elastic range could incorrectly affect the results of the analysis.

DAMAGE PARAMETERS

Initially, finite element meshes were defined for the concrete blocks and the mortar specimens, Figure 6. The lower base of the models was fully restrained; at the top of the models, the displacements that simulated the test loading scheme were applied along the vertical (Z) axis, whereas the horizontal displacements (along X and Y) were restrained to match the test conditions. Four-node tetrahedral finite elements were adopted for the mesh of the mortar specimens, whereas eight-node hexahedra were used for the block mesh, which requires a more defined description of the stress field. The number of elements was 663 and 1608, respectively, for the mortar specimen and for the concrete block.

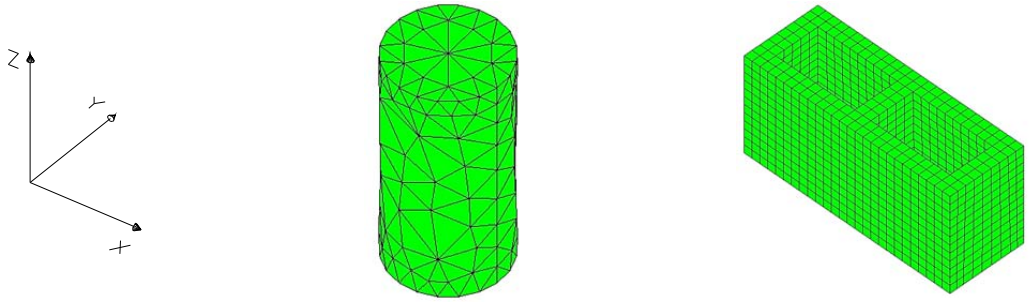

Figure 6: Finite element meshes: a) Mortar specimen; b) Block

The Young's modulus (E) and the Poisson coefficient (ν) were given the values identified during the experimental program for each component. The parameters A_c, B_c and y_{0c} that define the damage model in compression, see equation (2), were evaluated so that the representative load-displacement diagram experimentally obtained for each component, concrete block or mortar, would be closely matched by the numerical diagram for that component, Figure 7a and 7b. As for the parameters A_t, B_t and y_{0t} that define the behaviour of the materials in tension, the tests allowed only to evaluate the value for the blocks, Figure 7c. The values of the damage parameters for mortar in tension were assumed to coincide with those evaluated in compression. Indeed, as stresses in the mortar joint are mainly compressive due to the confinement of the material, the tensile behaviour of mortar is likely to play a negligible role, and the values given to A_t, B_t do not affect the numerical results significantly.

After assessing the local damage parameters it was possible to evaluate the spatial neighborhood radius (l_c) for the non-local damage model. In this paper this radius was considered as the smallest value for which the numeral procedure does not exhibit any strain localization. Table 1

summarizes the values of the damage parameters used to build the two-block prism model.

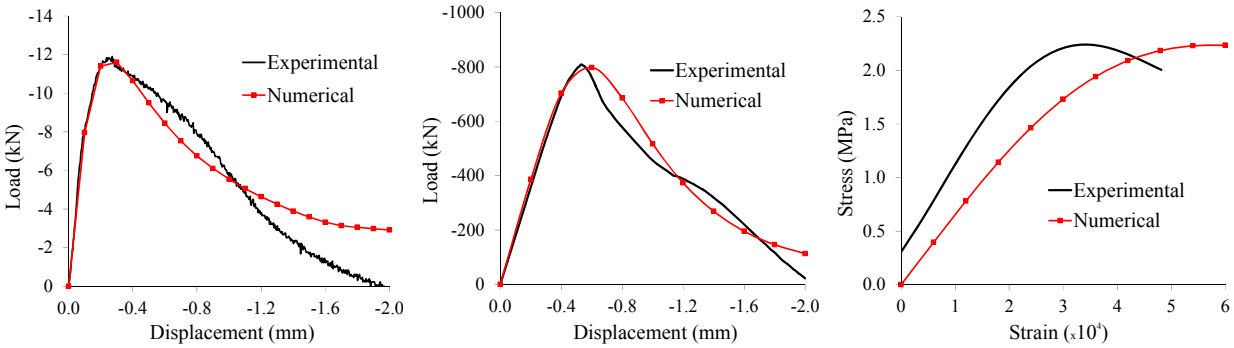

Figure 7: Damage Parameters - Compression: a) Mortar; b) Block – Tension: c) Block

Table 1: Damage Parameters

Component	E (MPa)	ν	y_{0c}	A_c	B_c	y_{0t}	A_t	B_t	l_c (mm)
Block	12800	0.20	1.0E+10	5.0E+08	1.7	1.0E+10	5.0E+08	1.2	150
Mortar	4790	0.20	1.0E+10	3.0E+05	1.0	1.0E+10	3.0E+05	1.0	50

NUMERICAL RESULTS FOR THE PRISM

The assembled mesh for the two-block prisms consists of 3484 eight-node hexahedral finite elements and is shown in Figure 8a. The parameters listed in Table 1 for the block and the mortar were used to model the prism. Similarly to the mortar specimen and the block models, the displacements along the axes X, Y and Z, were restrained both at the top and at the bottom of the meshes; the displacements that simulated the test loading scheme were applied along Z at the top of the model.

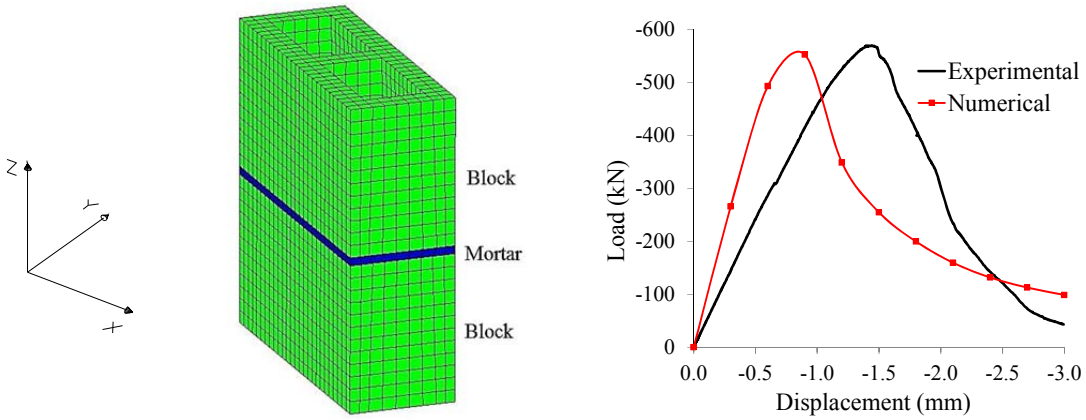

Figure 8: Prism model a) Mesh; b) Load/displacement diagram

A comparison between the experimental and numerical results is presented in Figure 8b and Table 2. It is possible to see that that the experimental and numerical results are quite close as far as the maximum load is concerned. As for the displacement at the peak load, the numerical value underestimates the experimental one, indicating that the numerical model was stiffer than the tested specimen. This can be due to the fact that the in-situ mechanical properties of the joint can

significantly differ from those obtained in the tests on the mortar specimens [11]. However, for the purpose of this work the numerical model can be considered adequately accurate.

Table 2: Maximum load and corresponding displacements for the prism

Maximum Load			Displacement at maximum load		
Numerical (kN)	Experimental (kN)	Diff. %	Numerical. (mm)	Experimental (mm)	Diff. %
552.4	570.1	-3.1	0.90	1,40	-35.7

Figure 9 and Figure 10 show contours of the damage variables at different steps of the analysis. Red refers to higher values of damage, and blue to lower values.

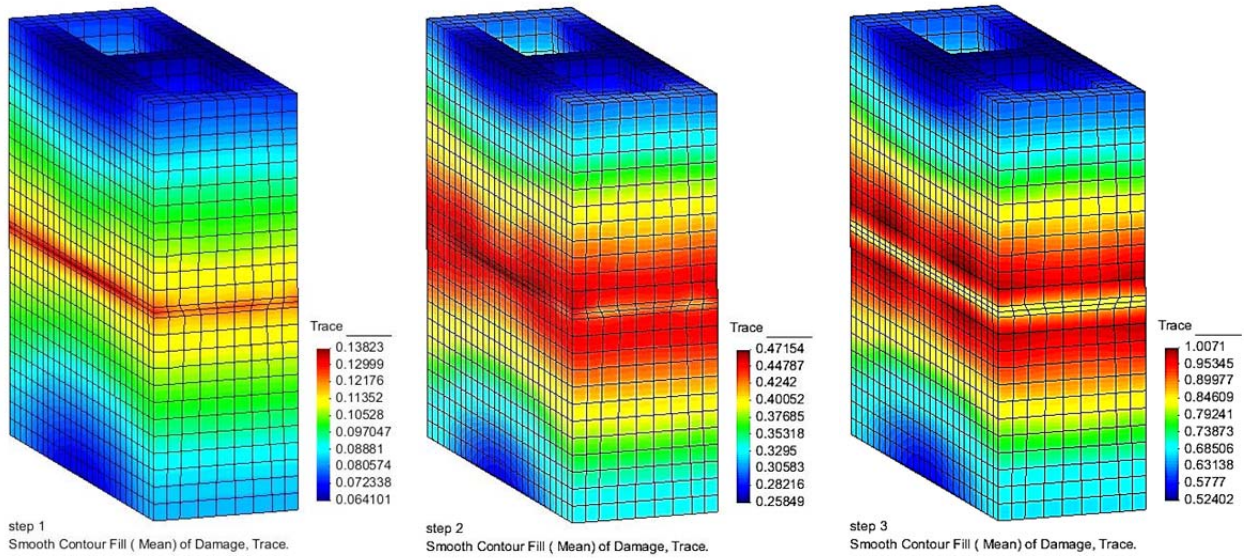

Figure 9: Trace of the damage a) step 1; b) step 2; c) step 3

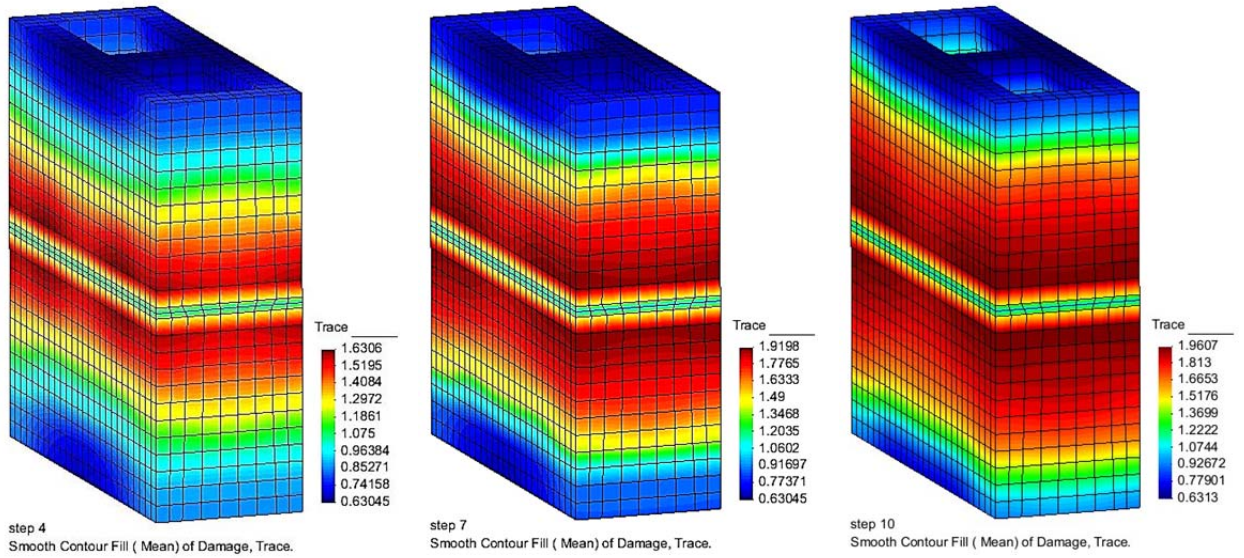

Figure 10: Trace of the damage a) step 4; b) step 7; c) step 10

Figures 9 shows the evolution of the trace of the damage tensor from step 1 to 3 (tr$\boldsymbol{D}$ = D_{11}+D_{22}+D_{33}). Step 3 corresponds to the peak load (see Figure 8b) and gives the damage values when the prism is about to fail. Figure 10 shows the trace of the damage from step 4 to 10, steps after the peak load. Step 10 is the last step of the numerical analysis, corresponding to a displacement of 3 mm.

Finally, Figure 11 shows contours of the individual damage components D_{11}, D_{22} and D_{33} at the last step of the analysis, step 10. The reference frame is shown at the upper right corner of the figure.

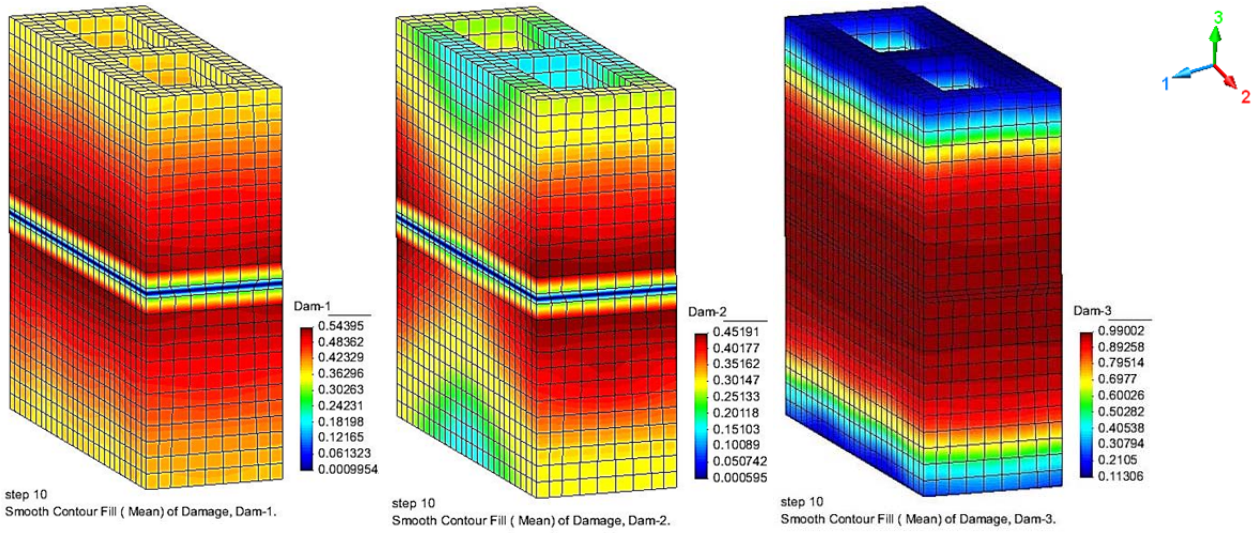

Figure 11: Damage at step no. 10 a) direction 1; b) direction 2; c) direction 3

PRISM FAILURE MODE AND COMPARISON WITH NUMERICAL RESULTS

Figure 12 shows the failure mode of the prism. The crack pattern observed in the experiment is in good agreement with that predicted by the numerical model. Indeed, according to Figures 9 and 10 where the damage evolution is shown, damage localizes mainly in the blocks at the two sides of the joint, conforming with the widespread cracking in these regions shown in Figure 12. Also, the spalling of concrete at the outer surfaces of the blocks is matched by the zones where D_{11} and D_{22} take higher values (see Figure 11). Note that damage develops also in the mortar joint (Figure 10c): in this case it consists in compressive damage along the vertical direction, which should be matched by crushing of the joints. It is not apparent from Figure 12 if crushing has actually occurred in the test: this point should be furtherly investigated.

CONCLUSIONS

The proposed numerical model was able to capture the main features of the mechanical behaviour of a concrete block masonry prism under compression with fair accuracy. Whereas the deformability of the prism is underestimated by the numerical predictions, the results of the proposed finite element model agree with the experimental findings in terms of peak load (i.e., of bearing capacity of the prism) and damage evolution, as the final crack pattern is matched by the regions where damage attains higher values.

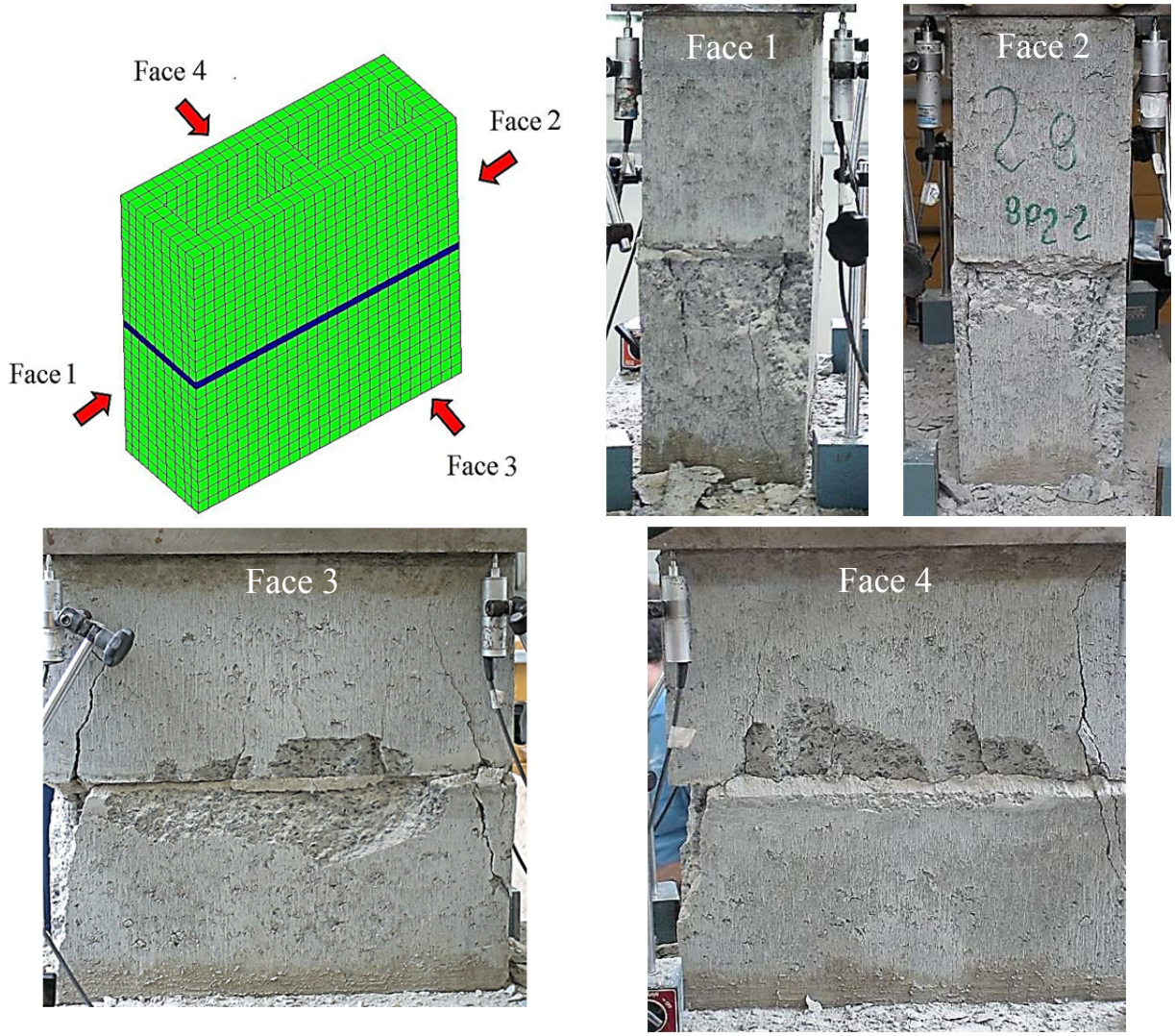

Figure 12: Failure mode of the prism

The availability of reliable numerical models to predict the global mechanical properties of masonry elements is of paramount importance, as time-consuming and expensive experimental tests can be avoided upon calibration of the model. In this work attention has been focused on the finite element modeling of a single prism, as current standards allow the carrying capacity of a block masonry wall to be predicted according to the results on prisms. Note, however, that stack bonded prisms do not represent the actual behaviour of walls in running bond: typically, they overestimate the actual allowable stress [12]. Thus, in the continuation of this research it would be worthwhile to numerically investigate the behavior of complex elements, which would be difficult to characterize experimentally, with the aim of correlating their mechanical response with that obtained from prisms made of hollow concrete blocks.

ACKNOWLEDGEMENTS

The authors gratefully acknowledge the support of FAPESP - São Paulo State Research Support Foundation and CNPq - National Council for Scientific and Technological Development. The

authors are also indebted to PhD's Alexandre Freitas and Rodrigo da Mata, who carried out the experimental activities presented in this work.

REFERENCES

1. Shrive, N.G., "The failure mechanism of face-bedded (ungrouted and unreinforced) masonry", Int. J. Masonry Constr., 2, 115-128, 1982.

2. Kachanov, L.M., "Time of the rupture process of non-linear solid mechanics", Otd. Tech. Nauk, 8, 28-31, 1958.

3. Rabotnov, Y.N., "Creep problems in structural members", North-Holland, Amsterdam, 1969.

4. Lemaitre, J., Chaboche, J.L., "Mechanics of solid materials", Cambridge University Press, Cambridge, UK, 1990.

5. Papa, E., Taliercio, A., "A visco-damage model for brittle materials under monotonic and sustained stresses", Int. J. Numer. Anal. Meth. Geomech., 29, 287-310, 2005.

6. Bažant, Z.P., Pijaudier-Cabot, G., "Nonlocal continuum damage, localization instability and convergence", J. Appl. Mech. (ASME), 55, 287-293, 1988.

7. Bažant, Z.P., "Instability, ductility, and size effect in strain-softening concrete", J. Eng. Mech. (ASCE), 102, 331-344, 1976.

8. Rodrìguez-Ferran, A., Morata, I., Huerta, A., "Efficient and reliable nonlocal damage models", Comput. Meth. Appl. Mech. Engrg., 193, 3431-3455, 2004.

9. Ramalho, M.A., Taliercio, A., Anzani, A., Binda, L., Papa, E., "A numerical model for the description of the nonlinear behaviour of multi-leaf masonry walls", Adv. Engng. Software, 39, 249-257, 2008.

10. Bažant, Z.P., Pijaudier-Cabot, G., "Measurement of characteristic length of non local continuum", J. Eng. Mech. (ASCE), 115, 755-767, 1989.

11. Vermeltfoort, A.T., van der Pluijm, R., "Strength and deformation properties of masonry to be used in computer calculations", Proc 9th Int. Brick/Block Masonry Conf., Berlin, 244-251, 1991.

12. Ganesan, T.P., Ramamurthy, K., "Behaviour of concrete hollow-block masonry prisms under axial compression", J. Struct. Eng. (ASCE), 118, 1751-1769, 1992.